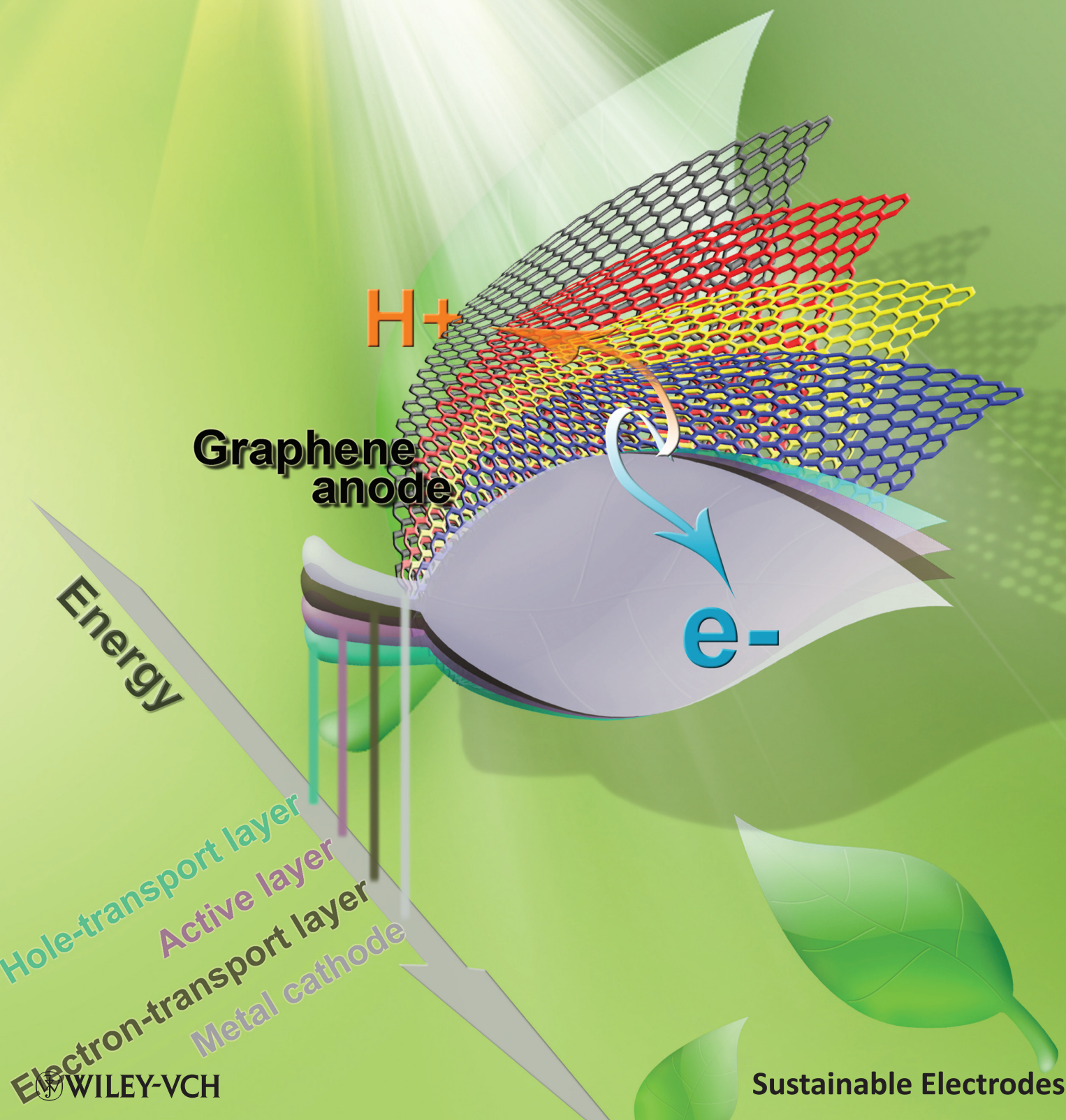


ADVANCED MATERIALS



Interface Engineering of Layer-by-Layer Stacked Graphene Anodes for High-Performance Organic Solar Cells

Yu Wang, Shi Wun Tong, Xiang Fan Xu, Barbaros Özyilmaz, and Kian Ping Loh*

The major efforts in solar energy research are currently directed at developing cost-effective systems for energy conversion and storage.^[1–3] The high cost of materials and preparation methods that are required for the fabrication of inorganic solar cells prevent their widespread deployment. Seeking a low-cost alternative in the form of solution-processable or roll-to-roll printable organic solar cells features prominently in the energy research roadmap. The conventional anode of choice for organic solar cells has been indium tin oxide (ITO), which consumes as much as 30% of the fabrication cost in solar cells. High quality ITO is expensive due to the dwindling supplies of indium. ITO also suffers from drawbacks like brittleness, sensitivity to acids and bases during processing, and reactive interface formation with copper indium sulfide during high-temperature sintering. Graphene films have been proposed as the new generation of multifunctional, transparent, and conducting electrodes. The attractiveness of graphene arises from their low cost, transparency, high electrical conductivity, chemical robustness, and flexibility, as opposed to the rising cost and brittleness of ITO.^[4–6] In particular, the 2D graphene sheet is emerging as a possible substitute for ITO in flexible displays, touch screens, and solar cells.^[7–9] The sheet resistance of graphene is given by $R_s = (\sigma_{2D} N)^{-1}$ where σ_{2D} is the 2D sheet conductivity and N is the number of layers. The intrinsic sheet resistance of single layer graphene is calculated to be $\approx 6 \text{ k}\Omega$ and is inferior to that of ITO ($10\text{--}20 \text{ }\Omega \text{ sq}^{-1}$).^[10] In principle, increasing the thickness (increasing N) of graphene using layer-by-layer stacking and doping the graphene (increasing σ_{2D} by increasing the carrier concentration) can allow the extrinsic sheet resistance values to be reduced to as low as $20 \text{ }\Omega \text{ sq}^{-1}$ although it is not trivial to reach this limit at present.^[10] Many are excited about the transparency and conductivity of multilayered graphene films, however the ultimate performance of graphene in solar cells may be limited by other factors. First, the interfacial energy offset between graphene and the photoactive materials has to be tuned in order to optimize charge transfer. Second,

the planarity and hydrophilic character of multilayer graphene has to be improved to allow for spin-coating with hole-transporting layers such as poly(3,4-ethylenedioxythiophene):poly(styrenesulfonate) (PEDOT:PSS). Third, the preparation of the graphene films has to be improved in terms of achieving large grain crystal growth, as well as reducing contaminations from organic residues in the transfer process. The organic residues have a deleterious effect on the conductivity, transparency, and roughness of graphene films. To date, there have been no reports that graphene can exhibit a power conversion efficiency (PCE) higher than ITO when replacing the latter in solar cell devices.^[11] This underscores the difficulty in optimizing any factors in the fabrication of the solar cell devices. It is timely to investigate the interface engineering of graphene in the context of high-performance solar cells. In this work, we carry out a systematic study of the different modification methods for graphene sheets with the aim of optimizing its role as an anode of solar cell. In this context, we have developed a direct layer-by-layer (LBL) transfer method of graphene sheets that is free from the residual impurity (poly(methyl methacrylate) (PMMA)) between the layers. Most importantly, by engineering the interface between the graphene film and the hole transfer layer, we have attained $\approx 83.3\%$ of the PCE of control devices based on ITO as anode. The interface engineering developed here is highly relevant for realizing photovoltaic (PV) and organic light-emitting diode (OLED) devices using graphene electrodes.

A single layer of graphene does not have sufficiently high sheet conductivity. Stacking multilayers together and doping them is needed to achieve higher extrinsic conductivity.^[12,13] Here, we propose a direct LBL interface coupling route for fabricating multilayer graphene films. A schematic diagram for the route is shown in **Figure 1a**. The difference between the reported route A and our LBL assembly method (route B) is this: as opposed to method A where the PMMA needs to be spin-coated and removed N times with the transfer of N layers, in method B, we only need to spin-coat the first layer graphene with PMMA once. In method B, the PMMA-coated graphene (first layer) is directly transferred onto the second layer graphene on copper foil. By annealing in $120 \text{ }^\circ\text{C}$ for 10 min, the $\pi\text{--}\pi$ interaction between the two layers of graphene bond them together. After etching the copper foil, the two-layer graphene film can be directly transferred onto a third layer graphene on copper foil, forming a three-layer graphene film. Based on these steps, N -layer graphene without any organic impurity between the layers can be obtained. Finally, the multilayer graphene can be transferred to other substrates, followed by the removal of the top PMMA in acetone. **Figure 1b** shows the LBL stacked graphene from 1 to 8 layers transferred onto quartz. The transmittance of the graphene film decreases with increasing number of layers

Y. Wang,^[†] S. W. Tong,^[†] Prof. K. P. Loh
Department of Chemistry
National University of Singapore
3 Science Drive 3, 117543, Singapore
E-mail: chmlhokp@nus.edu.sg

X. F. Xu, B. Özyilmaz
Department of Physics
National University of Singapore
2 Science Drive 3, 117542, Singapore

[†] Y.W. and S.W.T. contributed equally to this work.

DOI: 10.1002/adma.201003673

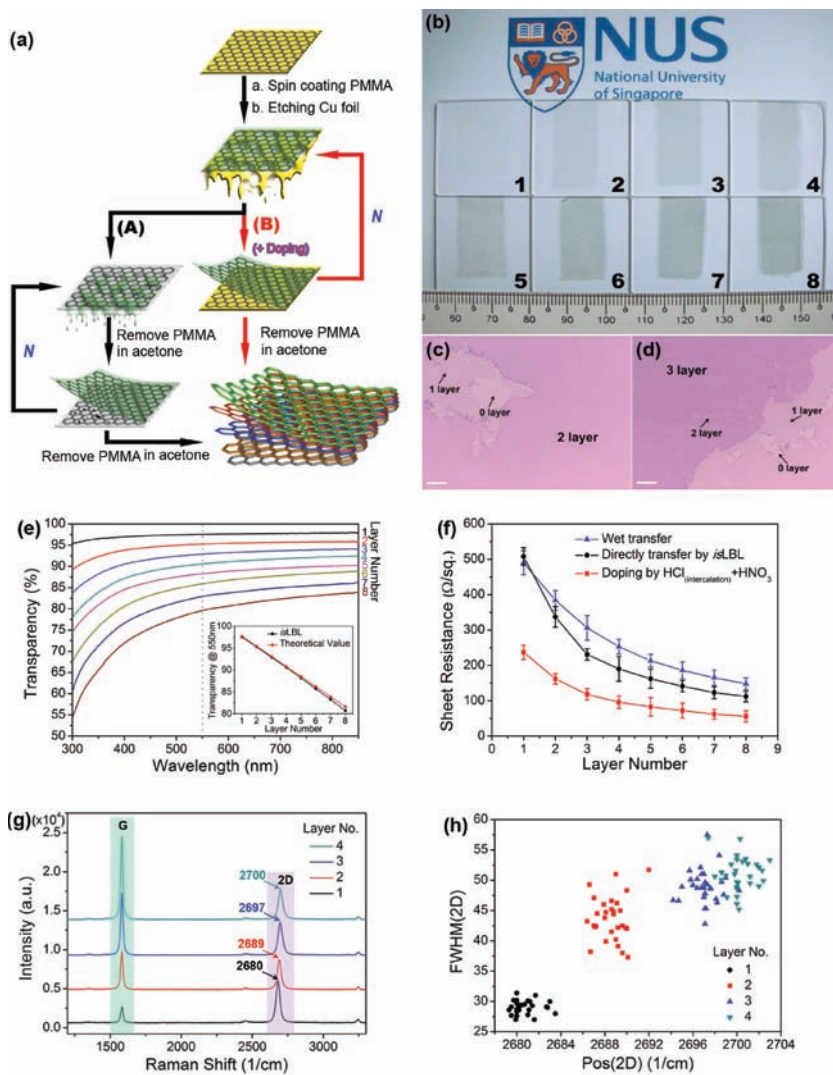


Figure 1. a) Schematic drawing of multilayer graphene films made by normal wet transfer (A) and direct coupling LBL assembly (B) ($N = 0, 1, 2, 3, \dots$). b) Optical image of multilayer graphene films (from 1 to 8 layers) on a quartz substrate. c, d) Typical optical microscope images of 2- and 3-layer graphene films on SiO₂/Si substrates. e) UV-vis spectra of LBL graphene films with 1 to 8 layers on quartz. The inset compares the transparency of the LBL film and its theoretical values at 550 nm. f) Comparison of sheet resistance vs layer number for graphene films prepared using wet transfer, LBL, and LBL acid-doped methods. g) Raman spectra of graphene films with 1 to 4 layers. h) A statistical result of the Raman spectra of full width half-maximum (FWHM) (2D) and peak position (2D) from 1 to 4 layers.

(Figure 1e). HCl is used to dope the individual layers during the transfer process, followed by HNO₃ doping at the surface of film after the removal of the top PMMA. The LBL, acid-doped, four-layer graphene film has a sheet resistance of $\approx 80 \Omega \text{ sq}^{-1}$ and a transmittance of $\approx 90\%$ at 550 nm. Generally, the sheet resistance of ITO with 80% transparency in the visible is less than $100 \Omega \text{ sq}^{-1}$ and flexible polyethylene terephthalate has a higher sheet resistance between $100\text{--}300 \Omega \text{ sq}^{-1}$.

The crystalline quality of the LBL stacked graphene films was analyzed by Raman spectroscopy (514 nm). It can be observed in Figure 1g that the defect-related D-band around 1350 cm^{-1} is negligible. Although the G-band frequency

at 1581 cm^{-1} is not affected by the assembly on the whole, the intensity ratio of $I(\text{G})/I(2\text{D})$ from 1 to 4 layer increases from 0.4 to 2.7.

The blueshift in the Raman 2D band with increasing layer is associated with the reduction in the Fermi velocity of the stacked graphene sample. Different twist angles between layers will affect the Fermi velocity differently, resulting in different degrees of blueshifting for the 2D band (Figure 1h).^[14] The 2D band of the LBL assembly graphene is also increasingly broadened from 1 to 4 layer, which should originate from the local, coupled interaction between the layers.^[15]

The as-grown graphene samples show standard bipolar field effect (Figure 2a) with a field-effect mobility of $5520 \text{ cm}^2 \text{ V}^{-1} \text{ s}^{-1}$ and $7780 \text{ cm}^2 \text{ V}^{-1} \text{ s}^{-1}$ at room temperature (300 K) and low temperature (1.6 K), respectively. The high mobility allows the observation of the quantum Hall effect (QHE). We can access the quantum Hall state when tuning the electron density by adjusting the gate voltage V_g at high magnetic field and low temperature. Figure 2b shows the longitudinal resistivity (ρ_{xx}) and the Hall resistivity (ρ_{xy}) of chemical vapor deposition (CVD) graphene as a function of the gate voltage at temperature (T) = 2 K and magnetic field (B) = 9 T. A series of half-integer plateaus with an integer filling factor $\nu = 2, 6, 10, 14,$ and 18 are clearly observed, which are the hallmark of the monolayer graphene. The unusual sequence of integer QH features is related to the quasi-relativistic nature of the charge carriers due to the particular graphene band structure near the Dirac point. In graphene, the conventional integer QH quantization for the resistivity ρ_{xy} is shifted by a half-integer due to the half-filling of the $n = 0$ Landau level compared to the other levels: $\rho_{xy} = \pm(h/4e^2)/(n+1/2) = h/\nu e^2$, where e is the elementary charge, n is the Landau level index, and h is Planck's constant. Despite the inhomogeneity of the carrier density when $\nu = 14$ and 18 , the Hall resistance plateaus at ρ_{xy} are robust and are accompanied by less prominent longitudinal resistance ρ_{xx} . The high mobility and QHE provides sufficient evidence for the high quality of such monolayer graphene samples.

To achieve high-performance organic solar cells, control of the surface free energy and work function of the electrodes is essential. In conventional poly(3-hexylthiophene-2,5-diyl):[6,6]-phenyl C₆₁ butyric acid methyl ester (P3HT:PCBM)-based polymer solar cell, PEDOT:PSS is spin-coated on top of the TO anode to prevent electron leakage and to aid in hole extraction. The active layer of P3HT:PCBM is sandwiched between an ITO/PEDOT:PSS anode and a low work function cathode. However, in the case of the graphene anode, PEDOT:PSS does

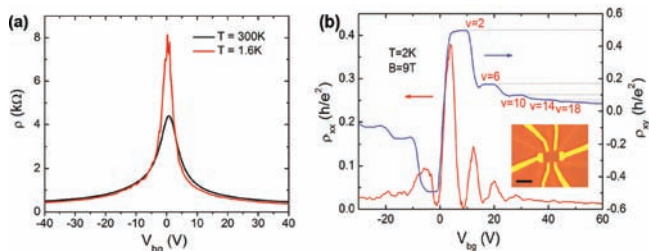


Figure 2. a) The field effect of the monolayer graphene with $B = 0$ T at room temperature ($T = 300$ K) and low temperature ($T = 1.6$ K). b) Quantum Hall effect at $T = 2$ K and $B = 9$ T for the same device. The first five half-integer plateaus with $\nu = 2, 6, 10, 14,$ and 18 , which are the fingerprint of single layer graphene, are clearly observed. An optical image of the typical device with Hall bar is shown in the insert. The scale bar is $3 \mu\text{m}$.

not spread well on the as-grown graphene due to its low surface free energy.^[16] To improve the hydrophilicity of graphene, a thin layer of (≈ 20 Å) molybdenum oxide (MoO_3) is evaporated on the graphene. The presence of the hydroxyl group on MoO_3 ^[17] allows the spreading of PEDOT:PSS on MoO_3 -coated graphene effectively. Ultraviolet photoelectron spectroscopy (UPS) measurements indicate that MoO_3 -coated graphene has a much higher work function (5.47 eV) than that of as-grown graphene (4.36 eV) (**Figure 3b**). The large increment in the work function of graphene is attributed to the high work function of MoO_3 (6.1 – 6.6 eV).^[18,19] As shown in the energy level diagram (**Figure 3c**), the work function of PEDOT:PSS^[20] and highest occupied molecular orbital (HOMO) level of P3HT^[21] is 5.2 eV, whilst the work function of MoO_3 -coated graphene is 5.47 eV. Thus the energy offset is favorable for barrierless hole extraction. In contrast, the large energy difference between the work function of as-grown graphene (4.36 eV) and the HOMO of P3HT (5.2 eV) introduces a barrier height of 0.84 eV for hole extraction.

The beneficial role of the MoO_3 +PEDOT:PSS interfacial layer in improving device performance of graphene anode was experimentally verified in solar devices using P3HT:PCBM as the photoactive layer. The device configuration is shown in **Figure 3a**. The performance of the LBL stacked (4 layers) graphene anodes, and the same but modified with either PEDOT:PSS only, MoO_3 only, or MoO_3 +PEDOT:PSS were compared to identify the best interface engineering methods. **Figure 3d** and **Table 1** (Supporting Information) indicates that the as-grown graphene device shows poor performance, with an open-circuit voltage (V_{oc}) of 0.5 V, short-circuit current density (J_{sc}) of 2.4 mA cm^{-2} , and fill factor (FF) of 0.29 , which yielded a low PCE of 0.35% . After modifying the graphene with MoO_3 +PEDOT:PSS double interfacial layer, a high V_{oc} value of 0.59 V was attained. Both J_{sc} (4.8 mA cm^{-2}) and FF (0.43) was also dramatically increased and produced an over threefold increment in PCE (1.23%).

Previously, Shrotriya et al. reported that the insertion of MoO_3 on ITO could increase V_{oc} from 0.49 V to 0.6 V.^[22] Similarly, the work function increment on MoO_3 -coated graphene can yield an improvement of V_{oc} . Similarly, we found that large V_{oc} value (0.59 V) can also be achieved in the MoO_3 modified graphene devices. The V_{oc} of polymer bulk heterojunction devices depends mainly on the bandgap (E_g) of the donor and acceptor. Vandewal et al. proposed with ohmic contacts at both the anode and cathode side.

$$V_{oc} \approx E_{g/e} - 0.43 \text{ V} \quad (1)$$

with ohmic contacts at both the anode and cathode side.^[23] Using 1.08 eV as the E_g value of annealed P3HT:PCBM layer,^[23] the estimated V_{oc} from Equation (1) is ≈ 0.65 V. It is quite close to the V_{oc} value (0.59 V) measured from the MoO_3 +PEDOT:PSS modified graphene device.

We observe that the double interfacial layer of MoO_3 and PEDOT:PSS is beneficial for the performance of the device. The MoO_3 islands can improve the hydrophilicity of graphene and thus assist PEDOT:PSS to wet the surface. The significance of this feature is verified by the performance of the graphene device using only PEDOT:PSS. Without the underlying MoO_3 , the structural inhomogeneity of PEDOT:PSS causes uneven charge extraction and results in a low PCE (0.12%). The photoactive layer deposited on non-uniform PEDOT:PSS will create a current leakage path and reduce the shunt resistance. Atomic force microscopy (AFM) shows that MoO_3 forms nanoislands on the graphene surface (see Supporting Information), so the device improvement should result from a combined work function improvement by MoO_3 and surface planarization effect on the deposited PEDOT:PSS. This planarization effect yields an improvement of both FF and J_{sc} .

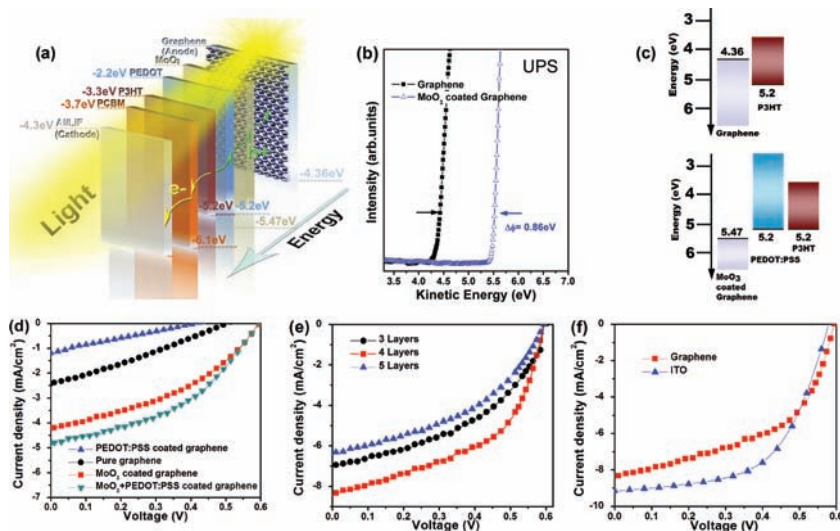


Figure 3. a) Schematic diagram of photovoltaic device structure. b) UPS spectrum showing the secondary cut-off of graphene before (black line) and after modification with MoO_3 (blue line). c) Energy level diagram at the anode side of the photovoltaic cells without (top) and with (bottom) the MoO_3 + PEDOT:PSS layer. d) Current density–voltage (J – V) characteristics of devices under light illumination. Anode/P3HT:PCBM/LiF/Al (anode = 4 layers as-grown graphene and the same coated by PEDOT:PSS only, MoO_3 only, or MoO_3 + PEDOT:PSS). e) 3–5 layers of acid-doped graphene/ MoO_3 +PEDOT:PSS/P3HT:PCBM/LiF/Al; f) anode/PEDOT:PSS/P3HT:PCBM/LiF/Al (anode is ITO or MoO_3 -coated graphene).

Further improvement in PCE can be achieved by acid-doping the graphene layer-by-layer to improve the extrinsic conductivity. Figure 3e and Table 2 (Supporting Information) show the PV effect of the devices with 3-layer, 4-layer, and 5-layer LBL-stacked graphene anode. The MoO₃+PEDOT:PSS double interlayer was applied to modify the graphene surface. As shown in Figure 3e, 4-layer acid-doped graphene solar cells exhibited the best PV performance in this work with PCE of 2.5%. A stable V_{oc} of 0.59 V, high J_{sc} of 7–8 mA cm⁻², and high FF of 0.45–0.51 could be obtained. Figure 3f compares the PV performance of this 4-layer graphene with a control device fabricated on ITO; the PCE of graphene is about 83.3% that of ITO. The control ITO device tested in our measurement conditions has a V_{oc} of 0.58 V, J_{sc} of 9.2 mA cm⁻², FF of 0.57, and PCE of 3%.

In principle, increasing the thickness of the film while not sacrificing transparency should produce a higher PCE due to its lower sheet resistance. However, the PCE decreases when we used 5-layer acid-doped graphene. In order to provide a deeper insight into the number of graphene films on the PV effects, series resistances (R_s) are analyzed. As reported by Choi et al.,^[24] R_s arises from the power loss of various resistive layers in solar cells and is given by

$$R_s A = P_R / J_{\max}^2 \quad (2)$$

where A is the active area, P_R is the total resistive power loss density, and J_{max} is the current density at the maximum power point while

$$P_R = P_{\text{anode}} + P_{\text{MoO}_3+\text{PEDOT:PSS}} + P_{\text{P3HT:PCBM}} + P_{\text{interfacial contacts}} + P_{\text{Al}} \quad (3)$$

where P_{anode}, P_{MoO₃+PEDOT:PSS}, P_{P3HT:PCBM}, P_{interfacial contacts}, P_{Al} are the resistive power loss densities of the interfacial contacts and different layers in the devices. Assuming good interfacial morphology is achieved between various layers in the devices, P_{interfacial contacts} will become negligible. P_{Al} can also be neglected because of the high conductivity of the Al cathode. Equation (3) can be further interpreted as

$$P_R = J_{\max}^2 (L^2 R_{\text{sheet_anode}}) / 3 + J_{\max}^2 (\rho t)_{\text{MoO}_3+\text{PEDOT:PSS}} + J_{\max}^2 (\rho t)_{\text{P3HT:PCBM}} \quad (4)$$

where R_{sheet_anode} is the sheet resistance of anode, L is the length of solar cell, ρ and t are the resistivity and thickness of the organic layers, respectively.

By combining Equations (2) and (4), R_s can be calculated as shown in Equation (5)

$$R_s A = (L^2 R_{\text{sheet_anode}}) / 3 + (\rho t)_{\text{MoO}_3+\text{PEDOT:PSS}} + (\rho t)_{\text{P3HT:PCBM}} \quad (5)$$

The results indicate that the values of R_s based on power loss are 14.9, 14.1, and 13.9 Ω cm² for 3, 4, and 5 layers of acid-doped graphene films, respectively. With the exception of the 5-layer graphene films, these R_s values are quite consistent with the values evaluated from the inverse slope of dark current density–voltage (J_D–V) characteristics of the real devices (see Supporting Information). The R_s values extracted from the inverse slope of J_D–V data are 15.5 and 14.6 Ω cm² for

3 and 4 layers graphene devices. Similar R_s values determined from two approaches further supports our initial hypothesis, i.e., good interfacial contacts exist in the devices. However, this assumption is invalid for graphene films that are >5 layers thick. The R_s values attained from J_D–V data of devices (21.5 Ω cm²) are much larger than that calculated from the power loss equations. The mismatched R_s values suggest that the total resistive power loss in the 5-layer graphene device is governed by the poor interfacial contact. In fact, we believe there is a trade-off between the sheet resistance and morphology in device performance. We have also investigated the PV effect of devices by replacing MoO₃ with pyrene buanoic acid succidimidyl ester (PBASE). 4-layer graphene anodes modified with PBASE also exhibited the highest PCE (2%) among other numbers of layers.

In conclusion, we demonstrate that the device efficiency of graphene-anode-based devices (2.5%) modified by MoO₃/PEDOT:PSS is very close to that of ITO-based devices (3%). Using 4-layer acid-doped graphene as the anode in organic solar cells, we have attained 83.3% of the PCE of ITO. In fact, all key photovoltaic parameters for solar devices fabricated using the graphene anode are quite similar to those of the ITO anode (Figure 3f). For further improvements to the PCE, the sheet resistance of graphene should be reduced. This can be accomplished either by more effective doping or by increasing the carrier mobility via interface control. One ongoing effort is to increase the size of the single crystal domain of CVD-grown graphene.^[25] The layer-by-layer stacking process of the graphene also needs to be improved. The main limitation at the present moment is the increasing roughness with the number of stacked layers in our film preparation process, which results in increased series resistance. Interface engineering of the graphene in terms of modifying its work function and surface free energy is also an important aspect in any charge or energy transfer device. By optimizing these processes, it is highly possible that the PCE of graphene will exceed that of ITO in organic or inorganic solar cell in due course. Finally, the unique advantages of graphene in terms of its flexibility, chemical robustness, and roll-to-roll processability can open a wide range of applications in flexible solar cell panels and display electronics that is not amenable to ITO.

Experimental Section

CVD Graphene: CVD graphene films were produced in a thermal CVD furnace using copper foil as substrate, similar to methods reported previously (see Supporting Information).^[13,26]

Fabrication of PV Devices: Sheet resistance values of graphene films were evaluated using four-point-probe method. The poly(3, 4-ethylenedioxythiophene):poly(styrene sulfonate) (PEDOT:PSS) film was first spin-coated on top of the anode (≈30 Ω sq⁻¹ ITO or MoO₃-coated graphene) and dried at 100 °C for 15 min. A 1000 Å P3HT:PCBM blend layer (1:0.8 w/w, 30 mg mL⁻¹) was then spin-coated from chlorobenzene on the PEDOT:PSS layer. LiF (10 Å) and Al metal (600 Å) were thermally evaporated through a shadow mask giving an active device area of 0.04 cm². To prepare MoO₃-modified graphene anode, 20 Å of MoO₃ was thermally evaporated through a shadow mask on the graphene film. After this, the devices were annealed on a hot plate at 120 °C for 10 min in the dry box. The fabricated solar cells were characterized with

a 150 W solar simulator with AM 1.5G filter from Newport Corporation at an intensity of 100 mW cm⁻². Previously, Shrotriya et al. reported the importance of selecting an appropriate reference cell for illumination intensity calibration.^[27] In order to report a reliable device efficiency value, we used a thermal detector with same spectral responsivity profile as that used in the work of Shrotriya et al. and the spectral mismatch was corrected.

Supporting Information

Supporting Information is available from the Wiley Online Library or from the author.

Acknowledgements

We thank the financial support of NRF-CRP award "Graphene and Related Materials and Devices" R-143 – 000-360 – 281.

Received: October 7, 2010

Revised: December 7, 2010

Published online: January 28, 2011

- [1] J. Y. Kim, K. Lee, N. E. Coates, D. Moses, T.-Q. Nguyen, M. Dante, A. J. Heeger, *Science* **2007**, 317, 222.
- [2] J. Peet, J. Y. Kim, N. E. Coates, W. L. Ma, D. Moses, A. J. Heeger, G. C. Bazan, *Nat. Mater.* **2007**, 6, 497.
- [3] T. Soga, *Nanostructured Materials for Solar Energy Conversion*, Elsevier, Amsterdam **2006**.
- [4] Z. Wu, Z. Chen, X. Du, J. M. Logan, J. Sippel, M. Nikolou, K. Kamaras, J. R. Reynolds, D. B. Tanner, A. F. Hebard, A. G. Rinzler, *Science* **2004**, 305, 1273.
- [5] X. Wang, L. Zhi, K. Müllen, *Nano Lett.* **2008**, 8, 323.
- [6] Y. Wang, X. H. Chen, Y. L. Zhong, F. R. Zhu, K. P. Loh, *Appl. Phys. Lett.* **2009**, 95, 063302.
- [7] S. Roth, H. J. Park, *Chem. Soc. Rev.* **2010**, 39, 2477.
- [8] Y. Xu, G. Long, L. Huang, Y. Huang, X. Wan, Y. Ma, Y. Chen, *Carbon* **2010**, 48, 3293.
- [9] L. G. De Arco, Y. Zhang, C. W. Schlenker, K. Ryu, M. E. Thompson, C. Zhou, *ACS Nano* **2010**, 4, 2865.
- [10] F. Bonaccorso, Z. Sun, T. Hasan, A. C. Ferrari, *Nat. Photonics* **2010**, 4, 611.
- [11] Y. M. Shi, K. K. Kim, A. Reina, M. Hofmann, L.-J. Li, J. Kong, *ACS Nano* **2010**, 4, 2689.
- [12] F. Güneş, H.-J. Shin, C. Biswas, G. H. Han, E. S. Kim, S. J. Chae, J.-Y. Choi, Y. H. Lee, *ACS Nano* **2010**, 4, 4595.
- [13] S. Bae, H. Kim, Y. Lee, X. Xu, J.-S. Park, Y. Zheng, J. Balakrishnan, T. Lei, H. R. Kim, Y. I. Song, Y.-J. Kim, K. S. Kim, B. Özyilmaz, J.-H. Ahn, B. H. Hong, S. Iijima, *Nat. Nanotechnol.* **2010**, 5, 574.
- [14] J. M. B. Lopes dos Santos, N. M. R. Peres, A. H. Castro Neto, *Phys. Rev. Lett.* **2007**, 99, 256802.
- [15] J. R. Wood, H. D. Wagner, *Appl. Phys. Lett.* **2000**, 76, 2883.
- [16] S. Wang, Y. Zhang, N. Abidi, L. Cabrales, *Langmuir* **2009**, 25, 11078.
- [17] T. S. Sian, G. B. Reddy, *Solid State Ionics* **2004**, 167, 399.
- [18] C.-T. Lin, C.-H. Yeh, M. -H. Chen, S. -H. Hsu, C.-I. Wu, T.-W. Pi, *J. Appl. Phys.* **2010**, 107, 053703.
- [19] Chen, I. Santoso, R. Wang, L. F. Xie, H. Y. Mao, H. Huang, Y. Z. Wang, X. Y. Gao, Z. K. Chen, D. Ma, A. T. S. Wee, W. Chen, *Appl. Phys. Lett.* **2010**, 96, 213104.
- [20] T.-W. Lee, Y. Chung, *Adv. Funct. Mater.* **2008**, 18, 2246.
- [21] J. Y. Kim, S. H. Kim, H. H. Lee, K. Lee, W. L. Ma, X. Gong, A. J. Heeger, *Adv. Mater.* **2006**, 18, 572.
- [22] V. Shrotriya, G. Li, Y. Yao, C.-W. Chu, Y. Yang, *Appl. Phys. Lett.* **2006**, 88, 073508.
- [23] K. Vandewal, A. Gadisa, W. D. Oosterbaan, S. Bertho, F. Banishoeib, I. V. Severen, L. Lutsen, T. J. Cleij, D. Vanderzande, J. V. Manca, *Adv. Funct. Mater.* **2008**, 18, 2064.
- [24] S. Choi, W. J. Potscavage, B. Kippelen, *J. Appl. Phys.* **2009**, 106, 054507.
- [25] X. S. Li, C. W. Magnuson, A. Venugopal, J. H. An, J. W. Suk, B. Y. Han, M. Borysiak, W. W. Cai, A. Velamakanni, Y. W. Zhu, L. F. Fu, E. M. Vogel, E. Voelkl, L. Colombo, R. S. Ruoff, *Nano Lett.* **2010**, 10, 4328.
- [26] X. S. Li, W. W. Cai, J. H. An, S. Kim, J. Nah, D. X. Yang, R. Piner, A. Velamakanni, I. Jung, I. E. Tutuc, S. K. Banerjee, L. Colombo, R. S. Ruoff, *Science* **2009**, 324, 1312.
- [27] V. Shrotriya, G. Li, Y. Yao, T. Moriarty, K. Emery, Y. Yang, *Adv. Funct. Mater.* **2006**, 16, 2016.

Copyright WILEY-VCH Verlag GmbH & Co. KGaA, 69469 Weinheim, Germany,
2010.

ADVANCED MATERIALS

Supporting Information

for *Adv. Mater.*, DOI: 10.1002/adma.201003673

Interface Engineering of Layer-by-Layer Stacked Graphene
Anodes for High-Performance Organic Solar Cells

Yu Wang, Shi Wun Tong, Xiang Fan Xu, Barbaros
Özyilmaz, and Kian Ping Loh *

Supporting Information

CVD growth of graphene: In a typical experiment, the CVD growth of graphene was carried out in a quartz tube at reduced pressure. Before the growth of graphene, copper foil (25 μ m thick, 99.999% purity) was pretreated at 1000 $^{\circ}$ C for 30min under a combined flow of Ar:H₂=50:10 in order to obtain the copper crystal with larger grain size. After that, Ar gas is replaced into high purity of methane (99.999%). A gas mixture of CH₄ (110 sccm) and H₂ (10 sccm) was used for the growth of graphene at \sim 5.0 Torr. After 30 min of growth, the system was cooled down to room temperature under H₂.

Characterization: The Raman spectra were measured using a WITEC CRM200 Raman system at room temperature. The excitation source is 532 nm laser (2.33 eV) with a laser power below 0.1 mW to avoid laser induced heating of the sample.

For resistance measurement, we apply a small AC current (10 nA) through the samples and measure longitudinal and transverse voltage using Stanford 830 lock-in amplifier. The samples were made into Hall bar geometry by standard e-beam lithography technique with the length of 3.5 micrometer between source and drain. A highly doped silicon wafer is used as the gate electrode with a 300nm silicon oxide as the dielectric layer. The room temperature resistance is measured in a probe station (Alessi REL-4800). Low temperature magnetoresistance is measured in Cryogenic 9T High Field System with a temperature range from 1.6 to 300K.

TABLE 1. Performance of graphene-based photovoltaic cells. Device configuration is anode/P3HT:PCBM/LiF/Al (anode is as-grown graphene, MoO₃-coated, PEDOT:PSS-coated graphene and MoO₃+PEDOT:PSS-coated graphene).

Layer number	MoO ₃	PEDOT:PSS	V _{oc} [V]	J _{sc} [mA/cm ²]	FF	η [%]
4	--	--	0.50	2.4	0.29	0.35
4	√	--	0.59	4.2	0.40	1.01
4	--	√	0.42	1.2	0.24	0.12
4	√	√	0.59	4.8	0.43	1.23

TABLE 2. Performance of photovoltaic cells with acid-doped graphene. Device configuration is graphene/MoO₃+PEDOT:PSS/P3HT:PCBM/LiF/Al.

Layer number	Interlayer doping	Surface doping	V _{oc} [V]	J _{sc} [mA/cm ²]	FF	η [%]
3	HCl	HNO ₃	0.59	7.0	0.45	1.9
4	HCl	HNO ₃	0.59	8.5	0.51	2.5
5	HCl	HNO ₃	0.59	6.4	0.44	1.6

TABLE 3. Performance of photovoltaic cells with ITO anode or graphene anode. Device configuration is anode/PEDOT:PSS/P3HT:PCBM/LiF/Al.

Anode	V _{oc} [V]	J _{sc} [mA/cm ²]	FF	η [%]
ITO	0.58	9.2	0.57	3.0
Graphene	0.59	8.5	0.51	2.5

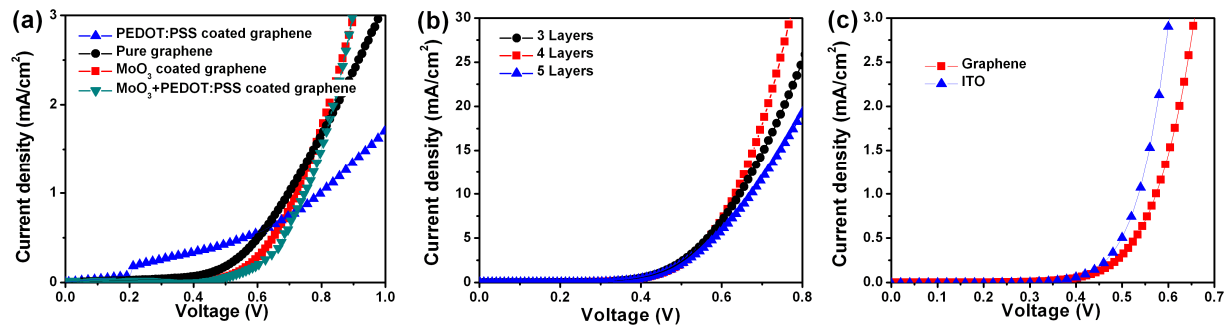


Figure S1. *J-V* characteristics of devices under dark condition (a) anode/P3HT:PCBM/LiF/Al (anode is 4 layers as-grown graphene, PEDOT:PSS coated or MoO₃ coated or MoO₃+PEDOT:PSS coated 4 layers as-grown graphene), (b) 3-5 layers of HCl+HNO₃-doped graphene/MoO₃+PEDOT:PSS/P3HT:PCBM/LiF/Al; (c) anode/PEDOT:PSS/P3HT:PCBM/LiF/Al (anode is ITO or MoO₃-coated graphene).

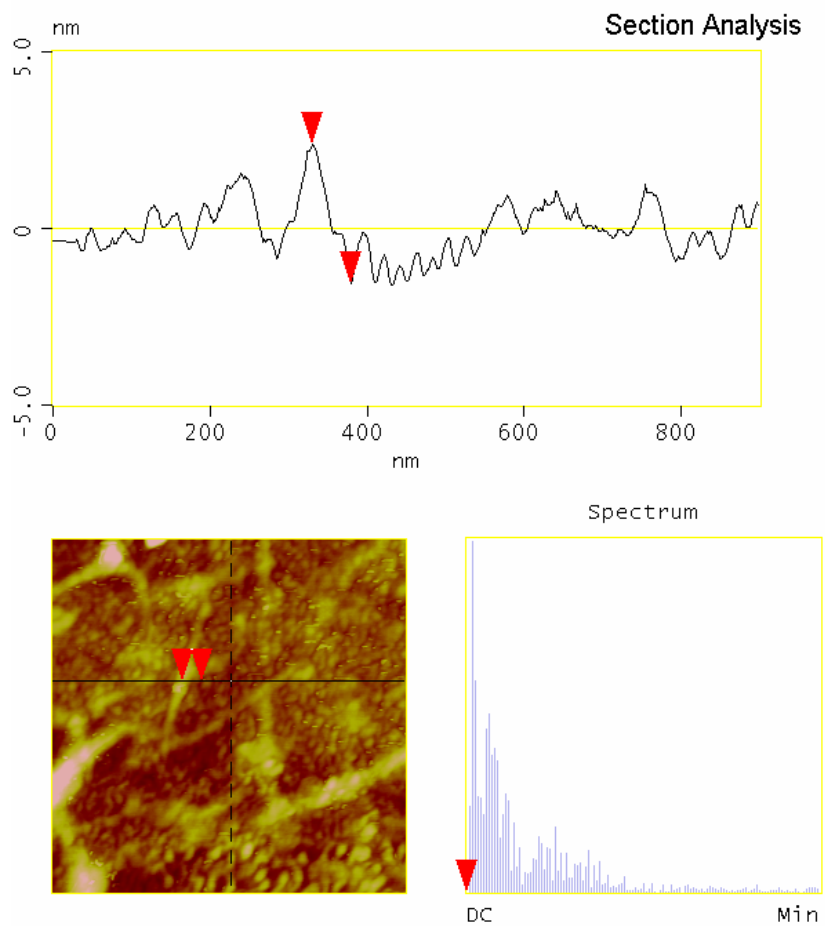


Figure S2. AFM sectional analysis of MoO₃-coated graphene. The MoO₃ forms nanoislands on graphene with the size of ~4nm.

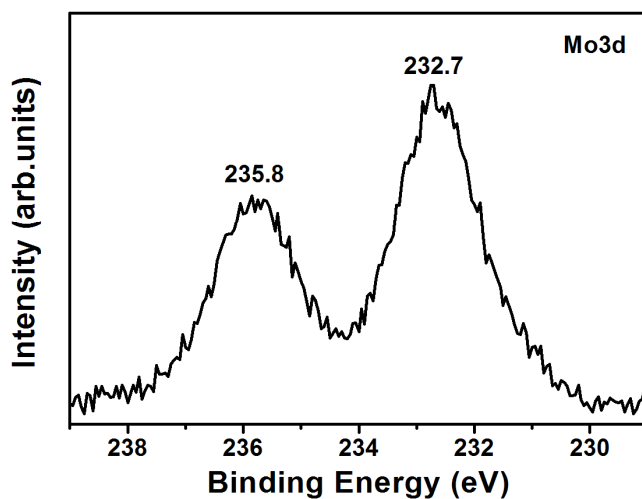


Figure S3. XPS Mo3d core-level spectrum of MoO₃-coated graphene. Peaks at the binding energy of 232.7 eV indicates that Mo ion exists as the (+6) form in MoO₃ film.

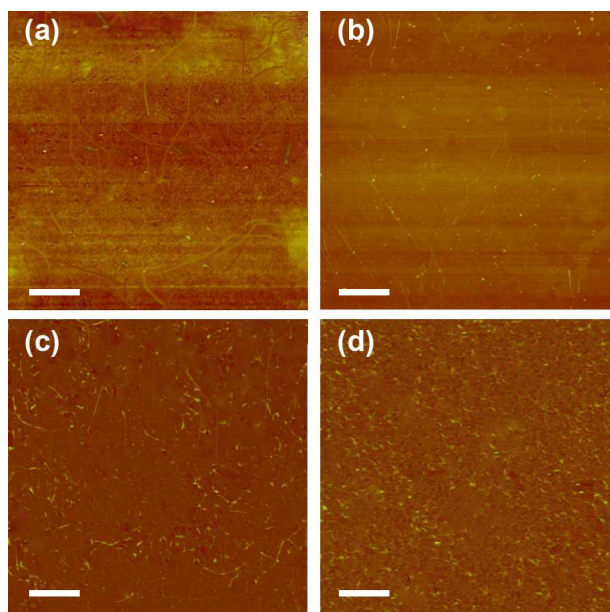


Figure S4. AFM images of graphene film with different layer number, (a) 2 layers, (b) 3 layers, (c) 4 layers, (d) 5 layers. Scale bar is 2 μ m.

TABLE 4. Root Mean Square (RMS) roughness vs. layer number of graphene film, showing the roughness increases with layer number of graphene.

Layer Number	RMS Roughness (nm)
2	1.22
3	2.31
4	3.88
5	5.62

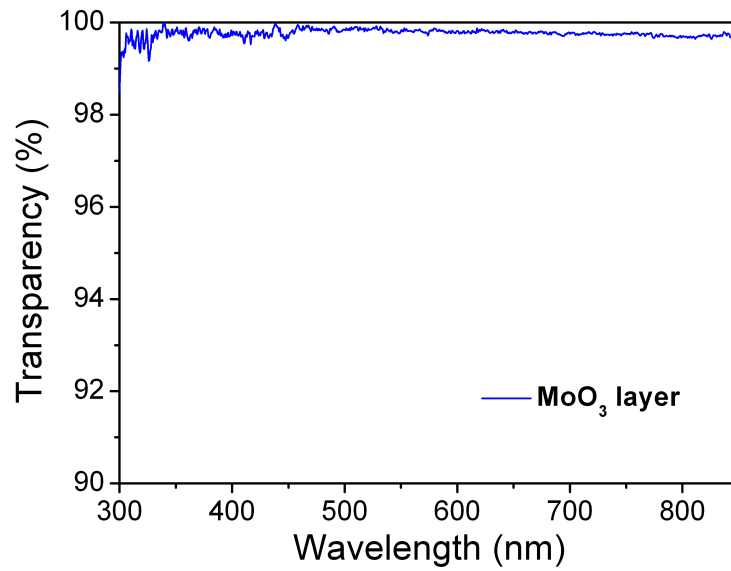


Figure S5. Optical transmittance spectrum of MoO₃ layer. The transmittance is over 99% between 300 to 850 nm.

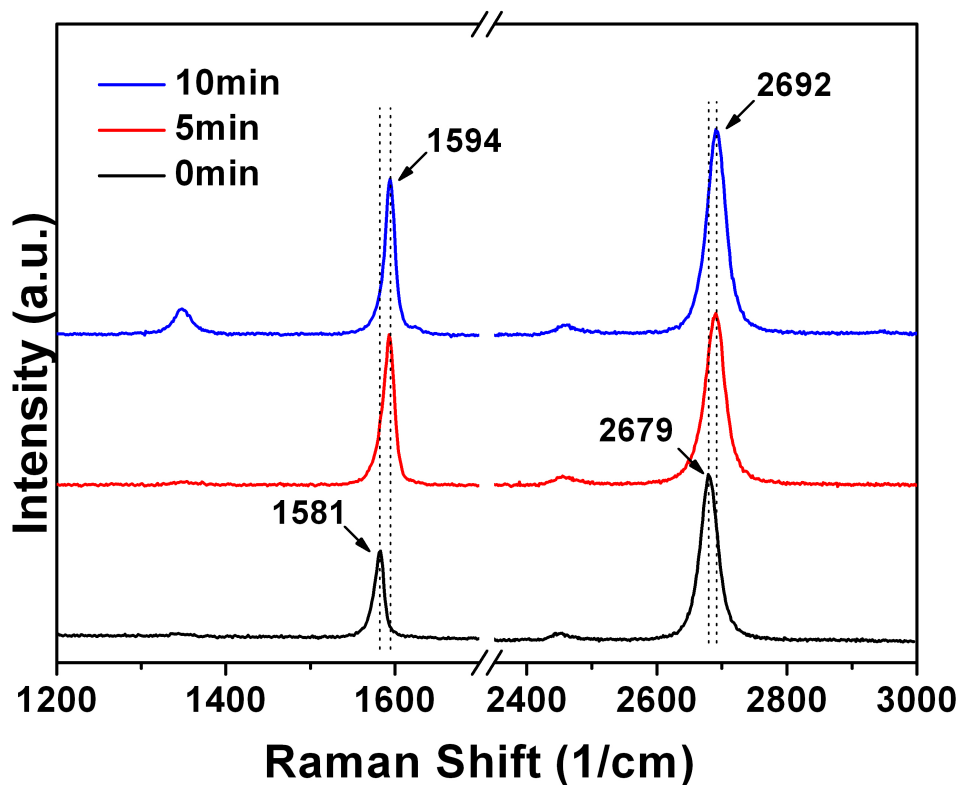


Figure S6. The Raman spectra of graphene films before and after HNO₃ doping. The *p*-doping results in a blueshift ($\sim 13 \text{ cm}^{-1}$) of both G and 2D peaks.